Irregular Photoinduced Electron Transfer between Doubly-Charged Pyrene and Alkali Metal Cations Studied by Fourier-Transform Electron Paramagnetic Resonance

Vladimir Rozenshtein, Gil Zilber, Mordecai Rabinovitz, and Haim Levanon*

Contribution from the Departments of Physical Chemistry and Organic Chemistry and the Farkas Center for Light-Induced Processes, The Hebrew University of Jerusalem, Jerusalem 91904, Israel

Received November 6, 1992

Abstract: Polarized FT-EPR spectra of photolyzed pyrene/alkali metal (Li, Na, K, Rb, Cs)/THF solutions were found to be time and alkali metal dependent. The polarization effects are initiated by electron transfer (ET) reactions between the doubly- and singly-charged pyrene (Py^{2-} and $Py^{\bullet-}$) and the alkali metal countercations (M^+). With the exception of Py/K/THF solution, the spin polarizations of all other systems, including those with a chelating agent added (cryptand), originate with a *triplet* precursor. The polarization is due to the action of several mechanisms: the correlated radical pair mechanism, $S-T_{-1}$ radical pair (RP) mixing, and the radical–triplet pair mechanism. However, in the Py/K/THF system, the polarization effects include different manifestations of the $S-T_0$ RP mechanism through exchange and dipole–dipole interactions with a *singlet*-state genesis. This irregular behavior is discussed in terms of the photoinduced ET reactions via the Marcus theory and by taking into account the competition between ET and intersystem crossing rates.

I. Introduction

A substantial number of photochemical reactions in liquids involve paramagnetic intermediates characterized by nonthermal spin distribution. Such nonequilibrated spin population arises from symmetry-driven molecular processes, such as singlet–triplet intersystem crossing (ISC). When detection time is short compared to relaxation times, electron spin polarization (ESP) effects, i.e., chemically induced dynamic electron polarization (CIDEP) and correlated radical pair mechanism (CRPM), can be easily monitored. CIDEP[1] consists of two basic mechanisms, namely the triplet mechanism (TM) and the radical pair mechanism (RPM). The latter includes $S-T_0$ and $S-T_{\pm1}$ mixing for the geminate RP (G-pairs) and free-pairing for encountering radicals (F-pairs). The effect of CRPM is usually found under restricted diffusion condition in viscous solutions,[2] micelles,[3] and biradicals.[4]

Most studies exhibiting ESP are carried out with systems in which photoexcited states are of neutral character. However, only a few experimental[5] and theoretical[6] investigations involve systems with Coulombic interaction of charged species. An attractive interradical potential can strongly affect the in-cage lifetime of the RP and, thus, reduce effectively the rate of diffusion (or escape) from the cage. In other words, since the RP cage size, r_C, is of a few angstroms, and if the value of the in-cage mutual diffusion coefficient, D, is smaller than that of free diffusion (10^{-5}–10^{-6} cm^2/s), then the magnitude of the diffusion times, t_d ($= r_C^2/D$), for the in-cage RP should be of the order of nanoseconds. These times are within the detection limits of time-resolved EPR spectroscopy, allowing direct observation of the RP in fluids with nearly normal viscosity.

In this work we have extended our recent qualitative time-resolved EPR study,[7] where photoejection of an electron from the pyrene dianion (Py^{2-}) in tetrahydrofuran (THF) solutions which contain different alkali metals,[8] produces polarized species that obey different ESP mechanisms. We have studied the effect of the ionic character of the RPs and their solvation properties, systematically and quantitatively, by employing alkali metals (M) in photoelectron-transfer reactions. We expect that ion pairing should result in reduction of in-cage diffusion rates and reveal specific CIDEP and CRP effects. To accomplish these goals, the systems described in section III were investigated, namely (1) solutions of Py/M/THF and (2) the same systems to which a chelating agent, cryptand (Kp), was added, i.e., Py/M/THF,Kp. These systems consist of dianions, Py^{2-}, ion-paired to the alkali metal countercations, M^+.[9] The experiments were carried out by utilizing selective pulsed-laser excitation combined with Fourier-transform (FT) EPR spectroscopy in the nanosecond time scale region.[7]

As we will demonstrate, the observed spin dynamics covers different CIDEP mechanisms and CRPM. By proper tuning of the Coulombic interaction and solvent properties via the specific alkali metal and solvation conditions, the various ESP effects can

(1) See, for example: (a) *Chemically Induced Magnetic Polarization*; Muus, L. T., Atkins, P. W., McLauchlan, K. A., Pedersen, J. B., Eds.; Reidel: Dordrecht, 1977. (b)Salikhov, K. M.; Molin, Yu. N.; Sagdeev, R. Z.; Buchachenko, A. L. *Spin Polarizations Magnetic Effects in Radical Reactions*; Elsevier: Amsterdam, 1984. (c)*Modern Pulsed and Continuous-Wave Electron Spin Resonance*; Kevan, L., Bowman, M. K., Eds.; Wiley: New York, 1990.

(2) (a) Tominaga, K.; Yamauchi, S.; Hirota, N. *J. Chem. Phys.* **1988**, *88*, 553. (b) Kroll, G.; Pluschau, M.; Dinse, K. P.; van Willigen, H. *J. Chem. Phys.* **1990**, *93*, 8709. (c) Yamauchi, S.; Ueda, T.; Satoh, M.; Akiyama, K.; Tero-Kubata, S.; Ikegami, Y.; Iwaizumi, M. *J. Photochem. Photobiol. A: Chem.* **1992**, *65*, 177.

(3) (a) Sakaguchi, Z.; Hayashi, H.; Murai, H.; I'Haya, Z. J.; Mochida, K. *Chem. Phys. Lett.* **1985**, *120*, 401. (b) Murai, H.; Sakaguchi, L.; Hayashi, H.; I'Haya, Y. J. *J. Phys. Chem.* **1986**, *90*, 113. (c) Closs, G. L.; Forbes, M. D. E.; Norris, J. R., Jr. *J. Phys. Chem.* **1987**, *91*, 3592. (d) Buckley, C. D.; Hunter, D. A.; Hore, P. J.; McLauchlan, K. A. *Chem. Phys. Lett.* **1987**, *135*, 307.

(4) (a) Closs, G. L.; Forbes, M. D. E. *J. Am. Chem. Soc.* **1987**, *109*, 6185. (b) Closs, G. L.; Forbes, M. D. E. *J. Chem. Phys.* **1991**, *95*, 1924. (c) Hasharoni, K.; Levanon, H.; Tang, J.; Bowman, M. K.; Norris, J. R.; Gust, D.; Moore, T. A.; Moore, A. L. *J. Am. Chem. Soc.* **1990**, *112*, 6477.

(5) Depew, M. C.; Wan, J. K. S. *J. Phys. Chem.* **1986**, *90*, 6597.

(6) (a) Pedersen, J. B.; Freed, J. H. *J. Chem. Phys.* **1974**, *61*, 1517. (b) Pedersen, J. B.; Freed, J. H. *J. Chem. Phys.* **1975**, *62*, 1790.

(7) Zilber, G.; Rozenshtein, V.; Levanon, H.; Rabinovitz, M. *Chem. Phys. Lett.* **1992**, *196*, 255.

(8) (a) Tuttle, T. R.; Weissman, S. I. *J. Am. Chem. Soc.* **1958**, *80*, 5342. (b) Ottolenghi, M.; Bar-Eli, K.; Linschitz, H. *J. Chem. Phys.* **1965**, *43*, 206. (c) Glarum, S. M.; Marshall, J. H. *J. Chem. Phys.* **1970**, *52*, 5555. (d) Dye, J. L. In: *Electrons in Fluids*; Jortner, J., Kestner, N. R., Eds.; Springer: Berlin, 1973; p 77

(9) (a) Holy, N. L. *Chem. Rev.* **1974**, *74*, 243. (b) Szwarc, M.; Levin, G. *J. Photochem.* **1976**, *5*, 119. (c) Rabinovitz, M. *Top. Curr. Chem.* **1988**, *146*, 99. (d) Rabinovitz, M.; Cohen, Y. *Tetrahedron* **1989**, *44*, 6957.

0002-7863/93/1515-5193$04.00/0

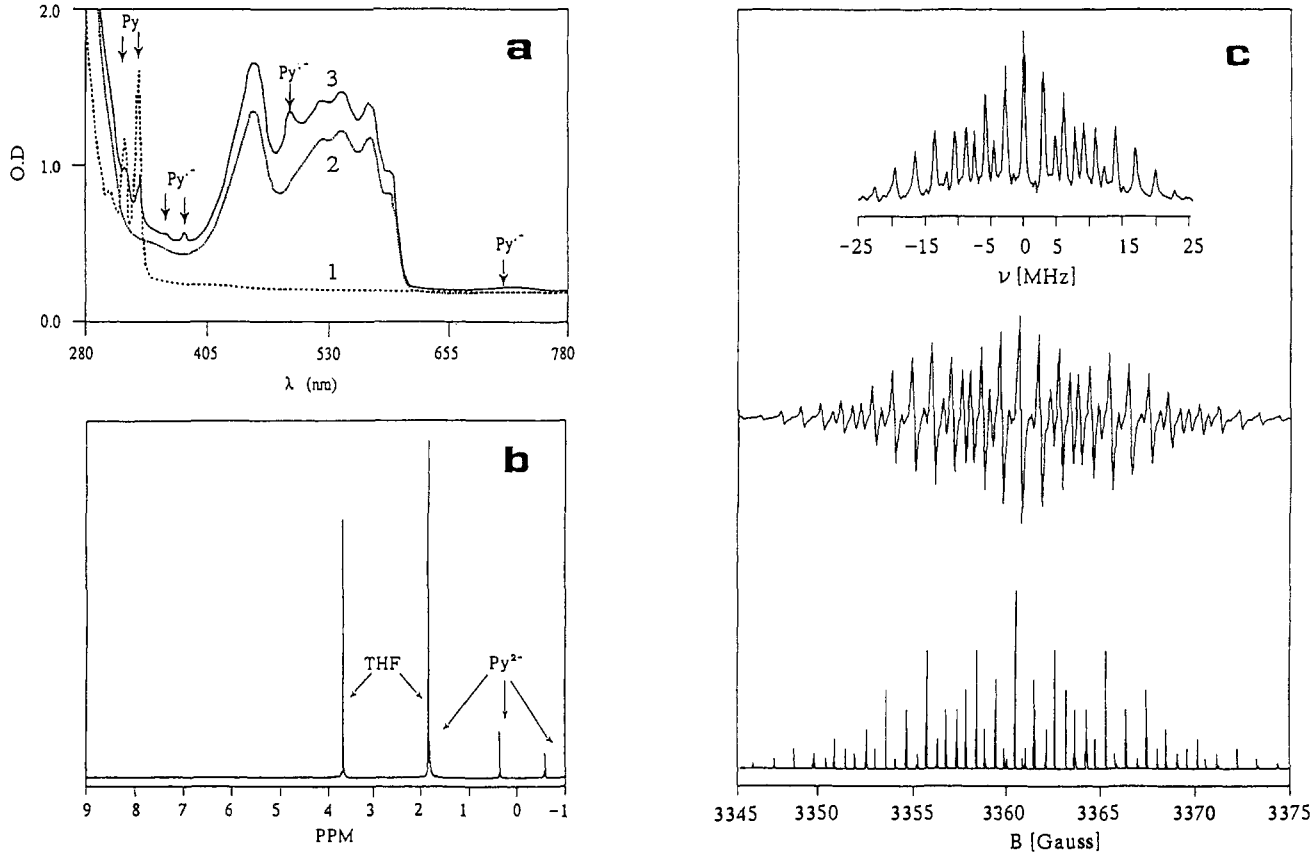

Figure 1. (a) UV–visible absorption spectra of Py solutions ($\sim 10^{-3}$ M): (1) Py/THF solution, (2) Py/Na/THF solution before light irradiation, and (3) Py/Na/THF solution after light irradiation. Arrows point out the Py and $Py^{\bullet-}$ absorption peaks. The other peaks relate to Py^{2-}. Similar spectra were obtained for the other metals (Li, K, Rb, Cs). (b) NMR spectrum of unirradiated Py/K/THF solution. (c) FT-, CW-, and stick EPR spectra of $Py^{\bullet-}$.

be controlled and differentiated. The results are discussed in section IV in terms of the nature of the ion pair complexes and of the different electron polarization mechanisms. Except for Py/K/THF system, all other systems exhibit similar ESP effects that are less dependent on the alkali metal. This unexpected result is discussed in terms of the relation between the free energy term, $\Delta G°$, and the nature of the precursor of the ET process between the charged pyrene and the alkali metal countercations. This dependence implies the identification of the inverted region of Marcus theory in these unique photoelectron-transfer reactions.

II. Experimental Section

EPR experiments were carried out using a commercial pulsed EPR spectrometer (Bruker ESP 380) interfaced to a pulsed (20 Hz, ~12-ns duration) Nd-YAG laser (Continuum, Model 661-2D). Light pulses (λ = 532 nm) of ~0.05 J/pulse (in some experiments up to ~0.2 J/pulse) were used. The FT-EPR spectra were taken in the X-band region ($\nu_0 \approx$ 9.22 GHz, $B \approx$ 3330 G), and all measurements were carried out at 167 K. Free induction decay (FID) signals were detected (using 24-ns microwave pulses) at selected delay times (τ_d) after the laser pulse. The minimum time between two successive slices of time-dependent FT-EPR spectra was 10 ns, determined by the digital oscilloscope (LeCroy, Model 9400A). The first time slices were taken for τ_d = 24 ns, i.e., for the overlap of the laser and microwave pulses. The FID dead time (t_{dt}) was about 130 ns in these experiments. In practice, for sufficiently strong signals one can observe the first-order kinetics of the magnetization decay (via spin lattice and chemical processes) corresponding to half-lives of $t_{dt}/5 \approx$ 25 ns.[10] The linear prediction singular value decomposition (LPSVD) routine[11] was applied for reconstruction of the FIDs within the dead time. This improved simultaneously the spectral and time resolutions, i.e., gathering information in 24 ns after laser excitation with 10-ns resolution between time slices. In every set of experiments we recorded a spectrum of the equilibrated pyrene radical anions, which was taken in the absence of light irradiation. These spectra were used as references for phase correction of the spin-polarized spectra. Pyrene, 2,2,2-cryptand (trade name Kryptofix, Kp), and THF (dried over Na/K alloy) were from Aldrich Chemicals. Dianions of pyrene (10^{-4}–10^{-3} M of parent concentrations) were prepared according to well-known procedures.[12] Each solution was checked prior to its photoexcitation by optical absorption, CW- (continuous wave) and FT-EPR, and NMR. These control experiments show that the main species present is Py^{2-}. Figure 1a displays the UV–visible absorption spectra taken for (1) Py/THF solution before reduction by the alkali metal, (2) Py/M/THF solution before irradiation, and (3) Py/M/THF system after exposing the sample to light irradiation (at 532 nm, absorbed by Py^{2-} only) for several minutes. The spectra show that the initial Py^{2-} turns partially into $Py^{\bullet-}$ and Py. Figure 1b depicts the NMR spectrum of nonirradiated solution.

III. Results

Except for Py/K/THF, all other systems exhibit very similar spectra. Therefore, in Figure 2 we show representative FT-EPR spectra of typical systems. Photolyzed solutions of Py^{2-} in the presence of Li and Rb in THF result in FT-EPR spectra which depend on τ_d (shown in Figure 2a,c). Figure 2b,d demonstrates the effect of added Kp on the spectra. The spectra of the Py/K/THF and the Py/K/THF,Kp system are shown in Figures 3a,b, and the former system clearly exhibits a dramatic change compared to all other systems. In every case, the final spectrum in Figures 2 and 3 (taken at the end of each experiment without light excitation) shows exactly the same line positions as those obtained for the FT-EPR spectrum of the stable pyrene radical anion, $Py^{\bullet-}$ (Figure 1c).[13,14]

A. Py/Li,Na,Rb,Cs/THF and Py/Li,Na,K,Rb,Cs/THF, Kp Systems. Examination of Figures 2 and 3 shows that, except for

(10) Norris, J. R.; Thurnauer, M. C.; Bowman, M. K. In *Advances in Biological and Medical Physics*; Lowrence, J. H., Gofman, J. W., Hayes, T. L., Eds.; Academic Press: New York, 1980; Vol. 17, p 365.

(11) Barkhuysen, H.; de Beer, R.; Bovée, W. M. H. J.; van Ormond, D. *J. Magn. Reson.* **1986**, *67*, 371.

(12) Paul, D. E.; Lipkin, D.; Weissman, S. I. *J. Am. Chem. Soc.* **1956**, *78*, 116.

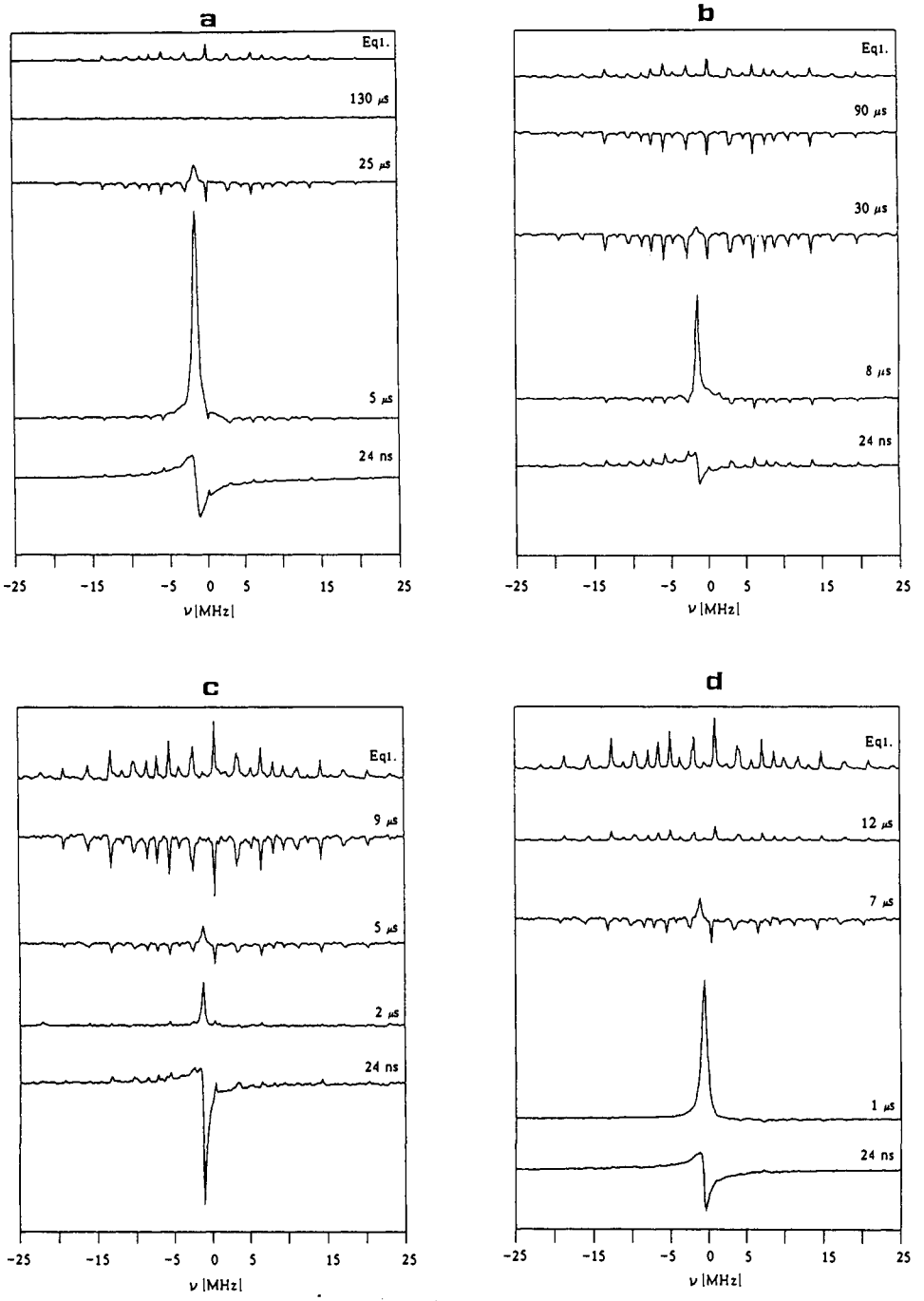

Figure 2. FT-EPR spectra vs delay time, τ_d: (a) Py/Li/THF; (b) Py/Li/THF,Kp; (c) Py/Rb/THF; (d) Py/Rb/THF,Kp. Notice that the frequency increase from left to right corresponds to a decrease of the magnetic field.

the Py/K/THF system, the spectral shapes are quite similar for all systems. In other words, the time-evolved spectra do not show a monotonous behavior that depends on the alkali metal size. Therefore, the systems will be described according to the spectral behavior at different times. The spectra in Figures 2 and 3b can be summarized as follows:

(i) In the time range of $0 < \tau_d < \tau_1$, the center line exhibits an absorption/emission (A/E) pattern which turns into a single absorption line above τ_1. The τ_1 value is different for each system and varies from 100 ns (Py/Rb/THF,Kp) to 500 ns (Py/Rb/THF) (cf. Figure 2). At this time interval, the A/E line is superimposed on a weak absorption spectrum of $Py^{\bullet-}$ that turns into emission later, above τ_1. In every case the emission part of the central derivative-like signal is more intense than its absorptive part. The peak-to-peak distance, $\Delta\nu_{pp}$, is the same for all systems and is equal to 0.7 ± 0.1 MHz for the first time slices. The absorption line, which stems from the derivative-like signal, has the same g value as its two-phase precursor (at the zero-intensity point on crossing the base line), $g = 2.0023 \pm 0.0002$, and line width approximately equal to $\Delta\nu_{pp}$ of the derivative-like (A/E) line.

(ii) Above τ_1, several time intervals should be considered: (1) For $Py^{\bullet-}$, $\tau_1 < \tau_d < \tau_2$, where the $Py^{\bullet-}$ spectrum appears in a pure emission mode. This evolves into an absorption mode at $\tau_d > \tau_2$

(13) (a) Hoijtink, G. J.; Townsend, J.; Weissman, S. I. *J. Chem. Phys.* **1961**, *34*, 507. (b) Segal, B. G.; Kaplan, M.; Fraenkel, G. K. *J. Chem. Phys.* **1965**, *43*, 4191. (c) Lyons, L. E.; Moore, J. E.; Morris, G. S. *Aust. J. Chem.* **1968**, *21*, 1337. (d) Anderson, M. E.; Pake, G. E.; Tuttle, T. R. *J. Chem. Phys.* **1960**, *23*, 1581. (e) Biehl, R.; Plato, M.; Möbius, K. *J. Chem. Phys.* **1975**, *63*, 3515.

(14) Spectra in Figure 1c were taken after completing the experiments without a further exposition of the sample to light. The stick spectrum in Figure 1c was simulated using the magnetic parameters $g = 2.0027$ and $a_1 = 4.80$G, $a_2 = -2.11$G, and $a_3 = -1.03$G.[13] We, therefore, attributed these spectra to an equilibrated state of $Py^{\bullet-}$. The difference in intensity distributions in Figure 1c is due to the limited bandwidth of the EPR spectrometer (~50 MHz).

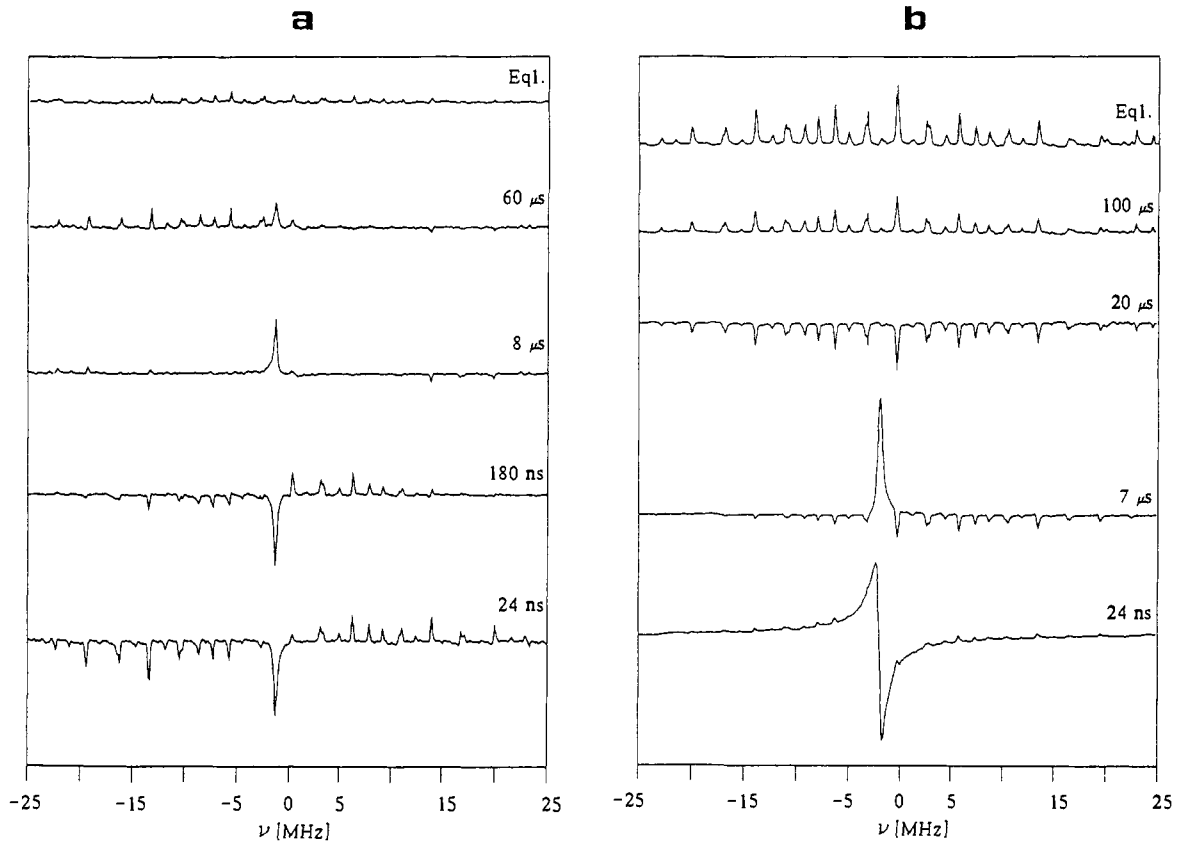

Figure 3. FT-EPR spectra vs delay time, τ_d: (a) Py/K/THF and (b) Py/K/THF,Kp solutions.

= 50–100 μs, giving the completely equilibrated $Py^{\bullet-}$ spectrum obtained at a few hundred microseconds (cf. Figures 2 and 3b for τ_2-values for each system). (2) For the single absorption line, with a lifetime of ~10–30 μs in all systems (cf. Figures 2 and 3b).

B. Py/K/THF System. The spectra of photoexcited Py/K/THF solution are inherently different from those described in the previous section. They consist of two time-dependent parts (see Figure 3a):

(i) In the time range $0 < \tau_d < 500$ ns, the spectra consist of two contributions, i.e., a multiplet ($g_1 = 2.0027 \pm 0.0002$) that exhibits an E/A polarization pattern and a central emissive single line ($g_2 = 2.0023 \pm 0.0002$). The former is assigned to $Py^{\bullet-}$, but the intensity distribution of its spectrum is strongly perturbed relative to the equilibrated spectrum. The $Py^{\bullet-}$ spectrum changes its sign at a microwave frequency corresponding to the g_2 value. The line width of the single line is about 0.3 ± 0.1 MHz.

(ii) At $\tau_d > 500$ ns, the multiplet and the single-line multiplet spectra change into an A/E polarization pattern for the former and A for the latter. The final step is equilibration which lasts up to ~200 μs.

IV. Discussion

The systems under investigation manifest different ESP mechanisms which appear at different τ_d. In-depth spectral analysis raises several key questions: (1) which ion pairs take part in the photoreactions, (2) which species produce the central single-line EPR spectrum, and (3) what is the origin of the ESP effects and the reason that the Py/K/THF system exhibits such a different behavior? The latter point is directly related to the question of which electron-transfer reactions occur in these systems and in what sequence.

A. Ion-Pair Complexes. The reduction by the alkali metals results in ion pairs in the following equilibria:[9]

$$M^{\bullet}_{solid} + Py \rightleftharpoons (Py^{\bullet-},M^+) \quad (1)$$

$$(Py^{\bullet-},M^+) \rightleftharpoons Py^{\bullet-} + M^+ \quad (2)$$

$$(Py^{\bullet-},M^+) + M^{\bullet}_{solid} \rightleftharpoons (M^+,Py^{2-},M^+) \quad (3)$$

$$2(Py^{\bullet-},M^+) \rightleftharpoons Py + (M^+,Py^{2-},M^+) \quad (4)$$

$$(M^+,Py^{2-},M^+) \rightleftharpoons (Py^{2-},M^+) + M^+ \quad (5)$$

During the sample preparation procedure, the above reactions are effective at the surface of the alkali metal mirror. When the solutions are out of contact with the metal surfaces, the main constituent is Py^{2-}, as verified by the UV–visible absorption, NMR, and ESR spectra of nonirradiated solutions (Figure 1). Thus, it is reasonable to assume that nonirradiated solutions contain two types of pairs, namely (M^+,Py^{2-},M^+) and (Py^{2-},M^+). These complexes exist as solvent-separated ion pairs (SSIP) or contact ion pairs (CIP).[15] The fraction of SSIP decreases with the increase of the countercation size.[15,16] Practically, one considers the complexes with Li^+ and Na^+ as SSIP and those with K^+, Rb^+, and Cs^+ as CIP. Since Kp is a powerful complexing agent, it can easily form SSIP.[17] Based upon MNDO calculations[18a] using lithium parameters,[18b] the structure and dimensions of the contact ion pair (Li^+,Py^{2-},Li^+) are shown in Figure 4a. The center-to-center distances between the localized negative charges in the aromatic rings and the alkali metal cations is ~2.2 Å, close to the sum of the ionic radius of Li^+ (0.6 Å)[15] and the accepted half-thickness value of an aromatic molecule (1.7–1.8 Å).[19] Since the metal–metal or metal–pyrene distances exceed considerably the radius of the alkali metal cation (the distances are determined

(15) Marcus, Y. *Ion Solvation*; Wiley: New York, 1985.
(16) (a) Hogen-Esch, T. E. *Adv. Phys. Org. Chem.* **1977**, *15*, 153. (b) Hogen-Esch, T. E. *J. Am. Chem. Soc.* **1966**, *88*, 307.
(17) Vögtle, F. *Supramolecular Chemistry*; Wiley: New York, 1991.
(18) (a) Dewar, M. J. S.; Thiel, W. *J. Am. Chem. Soc.* **1977**, *99*, 4899; **1977**, *99*, 4907. (b) Thiel, W. *QCPE* **1982**, *2*(438), 63; as icluded in MOPAC v 6.0 (Stewart, J. J. P. *QCPE 455* **1990**). (c) These calculations also provide the charge distribution, dipole moment, ionization potential, and triplet and singlet energies (E_T and E_S).
(19) (a) Pauling, L. *The Nature of the Chemical Bond*, 3rd ed.; Cornell: Ithaca, NY, 1960. (b) Jarvi, E. T.; Whitlock, H. W. *J. Am. Chem. Soc.* **1980**, *102*, 657.

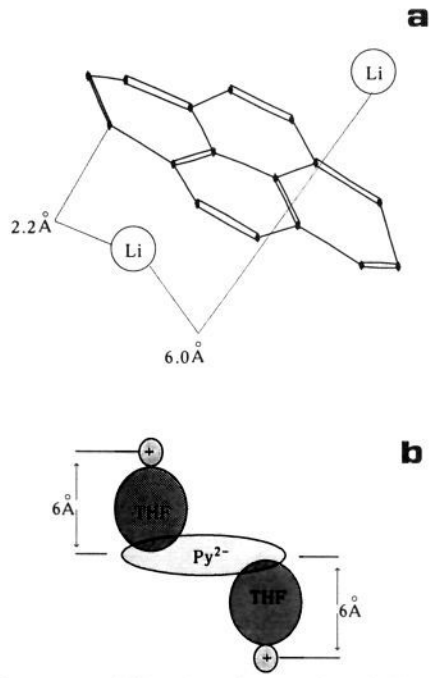

Figure 4. Structures and dimensions of contact ion pair (a) and solvent-separated ion pair (b). The line labeled 2.2 Å shows the distance between the lithium and carbon atoms, and the line labeled 6.0 Å shows the distance between the lithium atoms.

by charge distribution of the ion complexes), we may assume that the CIP of all alkali metals possess structures and parameters close to those of (Li^+,Py^{2-},Li^+). Also, it is reasonable to assume that the SSIPs have approximately the same structure as CIP but with solvent molecules inserted between the aromatic ring and the cations. Such SSIP is shown in Figure 4b, where the diameter of THF solvent molecule is assumed to be ~5–6 Å.[20]

B. Origin of the Single-Line EPR Spectrum. The single-line EPR spectrum is associated with the alkali metal atoms in solution. There are many measurements of g values and hyperfine coupling constants (hfc) of different alkali metal/solvent systems. These values differ from those of the free gas-phase atoms, with a strong dependence on the solvent and temperature.[21] Moreover, depending on the solvent, an EPR spectrum of the same alkali metal can appear as a single line or as a multiplet due to its nuclear spin.[22a,b,f]

In dilute solutions the equilibria involving the solvated species are[22]

$$M^+_s + e^-_s \rightleftarrows (M^+_s,e^-_s) \rightleftarrows M^{\bullet}_s \qquad (6)$$

The observed EPR spectrum is the time-averaged signal of e^-_s and $M^{\bullet}_s$ appearing on both sides of eq (6). Whether the signal is a single line or a multiplet can be determined by the values of two parameters, namely $P_s = \tau_c A_s$ and $P_m = \tau_m A_m$. The characteristic residence (or correlation) time for the electron in its solvation shells is τ_c, and A_s is the hfc between the unpaired electron and the solvent nuclei in the solvation shell. Similarly, τ_m and A_m are the lifetime and hfc of $M^{\bullet}_s$. The above parameters depend on the metal and the environmental conditions (solvent, temperature, etc.). Thus, upon increasing P_s and decreasing P_m, the tendency of a single-line spectrum dominates particularly at low temperatures. Probably, the presence of the dianion Py^{2-} in the vicinity of the metal cation enhances this tendency as well.

Formally, a situation in which the hfc varies by 2 orders of magnitude because of solvent or temperature is described by the multistate model.[22a] In this model the existence of a strong interaction between "the impurity" (the alkali metal atom) and "the host" (the solvent) results in the appearance of discrete states. These states are subjected to dielectric screening that reduces the Coulombic interaction, and the electron, which can be generated by photoexcitation of the organic dianion, moves into an expanded orbital about the metal cation. Donation of electron density from the host species (solvent molecules or counter anions) to the metal outer orbital produces delocalized electron density in the surrounding medium as well. These "impure" alkali metal states possess different hfc, ranging from 0 to the free-atom values. Populated states with low hfc are characterized by a single-line EPR spectrum. Such a spectrum of species with stoichiometry $M^{\bullet}_s$ suggests that the low unpaired electron spin density is on the metal nuclei. This is due to the dielectric screening of the solvent molecules (SSIP) and/or the pyrene species (CIP). As a result, the excited alkali metal atom is considered to be the loose ion pair ($M^{\bullet}_s{}^* \equiv M^+_s,e^-_s$). The above treatment is very similar to the Wannier–Mott model of exciton impurity states involving a correlated electron hole pair.[23] In the present context, the alkali metal cation plays the role of the positively charged hole.

An alternative view of the loose ion pair concept (M^+_s,e^-_s) in eq 6 arises from the electron jumps between the alkali metal and its surrounding molecules via random medium fluctuations. This causes a random modulation of the electron spin density on the nuclei and consequently a modulation of hyperfine interaction. If the characteristic exchange frequency exceeds the scale of the hfc of the EPR spectrum of $M^{\bullet}_s$, then the spectral components merge into a single narrow line. A different approach of interpreting the single-line spectrum is to compare the residence times of the free and bound electrons to the ratio of the line width of the single line and the hfc of $M^{\bullet}_s$.[25a] Thus, although equilibria 6 exist in our systems, under the present experimental conditions the spectra of $M^{\bullet}_s$ escape detection.[22]

C. Theoretical Aspects of Electron Spin Polarization. To answer the last question about the origin of the polarization effects, we will start with the different ESP mechanisms that might be operative in the interpretation of the time-evolved FT-EPR spectra.[24]

C1. Primary Excitation. Photoexcitation of Py^{2-} (eq 5) results in the following singlet states:

$$M^+,{}^1(Py^{2-}),M^+ \xrightarrow{h\nu} M^+,{}^1(Py^{2-})^*,M^+ \qquad (7)$$

$$M^+,{}^1(Py^{2-}) \xrightarrow{h\nu} M^+,{}^1(Py^{2-})^* \qquad (8)$$

These states can initiate the electron transfer reactions to the metal cations either directly or following intersystem crossing, producing the triplet states. The excited singlet and triplet are the precursors of the polarization mechanisms which will be briefly discussed below.

The most probable mechanism for the S–T mixing is the spin–orbit coupling, ω_{LS}, which, for planar π-hydrocarbon systems, is much bigger ($\omega_{LS} \sim 10^{11}$–10^{12} rad/s)[25] than the Zeeman and the hf interactions. In our case, the ISC routes are

$$M^+,{}^1(Py^{2-})^*,M^+ \xrightarrow{ISC} M^+,{}^3(Py^{2-})_p,M^+ \qquad (9)$$

$$M^+,{}^1(Py^{2-})^* \xrightarrow{ISC} M^+,{}^3(Py^{2-})_p \qquad (10)$$

where the subscript p stands for spin-polarized species. It should

(20) Derived from the molar volume value of 81.6 cm³/mol in sphere-shape approximation for this molecule.[15]

(21) *Landolt-Bornstein Numerical Data in Science and Technology, Atomic and Molecular Physics*; Springer-Verlag: Berlin, 1987; Vol. 17A.

(22) (a) Catterall, R.; Edwards, P. P. *J. Phys. Chem.* **1975**, *79*, 3010; **1975**, *79*, 3018. (b) Catterall, R.; Edwards, P. P. *Chem. Phys. Lett.* **1976**, *42*, 540. (c) Friedenberg, A.; Levanon, H. *Chem. Phys. Lett.* **1976**, *41*, 84. (d) Eliav, U.; Levanon, H. *J. Phys. Chem.* **1980**, *84*, 842. (e) Eliav, U.; Freed, J. H. *J. Phys. Chem.* **1984**, *88*, 1277. (f) Edwards, P. P. *J. Phys. Chem.* **1984**, *88*, 3772.

(23) (a) Frankevich, E. L. *Sov. Phys. JETP* **1966**, *23*, 814. (b) Rusin, B. A.; Frankevich, E. L. *Phys. Status Solidi* **1969**, *33*, 885. (c) Raz, B.; Jortner, J. *Chem. Phys. Lett.* **1970**, *4*, 511.

(24) To simplfy, we drop the subscript s indicating solvated species.

(25) (a) Weissman S. I., private communication. (b) Turro, N. J. *Modern Molecular Photochemistry*; Benjamin-Cummings: Menlo Park, 1978.

be noted that in our case, the rate of producing $^3(Py^{2-})_p$ does not exceed the rate of light absorption, $(\tau_L)^{-1}$, and if the condition $\tau_{ET}^{-1} \leq \tau_L^{-1}$ is satisfied, the triplet population can be comparable to the parent molecule concentration.[26] Here, τ_{ET} is the characteristic time of the ET process. The polarized triplets produced in processes 9 and 10 can be further involved in polarization effects, provided that these processes compete with the ET from the excited singlet of Py^{2-}.

C2. Triplet Mechanism. Following reactions 9 and 10, ET produces the radicals and radical ions:[27]

$$M^+,{}^3(Py^{2-})_p,M^+ \xrightarrow{ET_1} {}^3(M^\bullet_p,Py^{\bullet-}_p),M^+ \qquad (11a)$$

$$^3(M^\bullet_p,Py^{\bullet-}_p),M^+ \xrightarrow{ET_2} {}^3(M^\bullet_p,Py,M^\bullet_p) \qquad (11b)$$

$$M^+,{}^3(Py^{2-})_p \xrightarrow{ET_1} {}^3(M^\bullet_p,Py^{\bullet-}_p) \qquad (12)$$

In the case of TM, triplet polarization is transferred to the doublet states of the radicals $M^\bullet$ and $Py^{\bullet-}$, and the efficiency of TM is determined by: (1) the degree of selectivity of the triplet ← singlet ISC population rates described by eqs 9 and 10 and (2) the requirement that $\tau_{ET}^{-1} = k_{ET} > T_{1T}^{-1}$, where T_{1T} is the triplet spin-lattice relaxation time. Also, reactions 11 and 12, like the preceding processes (7–10), must occur during the laser pulse. The early time spectra of $Py^{\bullet-}$ (represented by the 24-ns spectra in Figures 2,3b) can be attributed to the polarized constituents in eqs 11 and 12. The contribution of TM to the spectrum of $M^\bullet$ is not seen because of the domination of other mechanisms (see below).

ISC, being driven by spin–orbit coupling, is independent of the nuclear spin. Therefore, the TM polarization lacks the hyperfine dependence. The TM creates a net polarization (p_{TM}), and both radicals possess the same polarization phase (absorption or emission) equal to:[28]

$$p_{TM} = k_{el}m_T/(k_{el} + T_{1T}^{-1}) \qquad (13)$$

where m_T is the total polarization of the triplet molecule, i.e.:

$$m_T \sim -D_{ZFS}[{}^1/_2(k_{xx} + k_{yy}) - k_{zz}] \qquad (14)$$

where D_{ZFS} is the zero-field splitting parameter and k_{ii} are the rate constants for ISC into the different triplet substates. Unfortunately, the triplet magnetic parameters of $^3(Py^{2-})$ in fluid THF are not available, and the experimental result, i.e., absorption (Figures 2 and 3b), is in line with $k_{zz} > {}^1/_2(k_{xx} + k_{yy})$ and $D_{ZFS} > 0$ or vice versa.[28d]

The RP, on the right-hand side of eq (12), can separate by diffusion, keeping its polarization in the absorption mode, followed by relaxation with characteristic times $T_{1R}(Py^{\bullet-})$ and $T_{1R}(M^\bullet)$ which are of the order of a few microseconds (cf. Figure 2c):

$$^3(M^\bullet_A,Py^{\bullet-}_A),M^+ \xrightarrow{diff} M^\bullet_A + (Py^{\bullet-},M^+)_A \xrightarrow{T_{1R}} M^\bullet + (Py^{\bullet-},M^+) \qquad (15)$$

$$^3(M^\bullet_A,Py^{\bullet-}_A) \xrightarrow{diff} M^\bullet_A + Py^{\bullet-}_A \xrightarrow{T_{1R}} M^\bullet + Py^{\bullet-} \qquad (16)$$

C3. Cage Effects and Restricted Diffusion. RPM in an unorganized liquid assumes that spin polarization is produced upon singlet–triplet mixing during diffusion of radicals[1] or within the RP cage, where an attractive interradical interaction exists and restricts the effective diffusional motion.[29] The characteristic lifetime of a RP depends on the mutual diffusion coefficient of the pair constituents.

In a separation, the motion of the pair is highly correlated, thus inducing a spatial dependence of the diffusion coefficient, which decreases as the particles approach each other.[30] This effect was experimentally demonstrated[31] in the reaction of triplet benzophenone (B) with *p*-cresol (PhOH) in glycerol. For the RP ($BH^\bullet$,$PhO^\bullet$), the coefficient of mutual diffusion, describing the geminate recombination of the neutral radicals, was found to be much smaller than the sum of the individual diffusion coefficients of these species (up to 1 order of magnitude). In addition, Coulombic and/or charge-induced dipole–dipole (as a result of electrical polarization of the radicals) interactions can also restrict the diffusion.[6,29] Indeed, the numerical[6] and analytical[29] solutions show that an attractive potential of a few kT (~0.1 eV) increases the lifetime of an interacting pair by a factor of ~20. Moreover, an ionic character of the RP should induce an increased probability of reencounters, which also increases the in-cage lifetime of the RP. Therefore, assuming that all cage effects are additive, we conclude that a RP of ionic character possesses a smaller mutual diffusion coefficient, by a factor of 100–1000, in comparison to the sum of the individual coefficients.

In terms of the Stokes–Einstein equation, we can estimate the conventional diffusion coefficient D:

$$D = kT/6\pi\eta r_0 \qquad (17)$$

where η is the viscosity coefficient of the solvent and r_0 is the sum of the van der Waals radii of the encounter particles. For THF at 167 K, $\eta = 6$ cP,[32] and for $r_0 = 6$ Å (cf. Figure 4) one obtains $D \approx 3 \times 10^{-7}$ cm²/s. Taking into account the above-mentioned restricted diffusion effects, we can estimate a D-value of $\sim 10^{-9}$ cm²/s for the RP under investigation with a characteristic diffusion time of $r_0^2/D \approx 5$ μs. This estimated value predicts the existence of quasiorganized structures, in which the diffusional motion (and also rotation) of the RP is suppressed. The unique properties of the solvated electron, considering temperature, viscosity, and the particular metal, also cause the $M^\bullet$ species to behave, in many respects, as the quasiindependent solvated electron. Within this context it is noteworthy that the studies of alkali metal solutions in ammonia, amines, and ethers have shown that the solvated electron on the left-hand side of eq 6 can be considered as the simplest anion radical, i.e., e^-_s, lacking the positively charged core. The "excess" electron is more or less equally shared among a number of solvent molecules, and the electron density is symmetrical about the center of a cavity of radius $r_e \approx 3$ Å in the solvent. The electron is self-trapped in this cavity and interacts

(26) Presently, for laser pulses of 12-ns duration time and energy of 0.05–0.2 J, light is absorbed within a time interval of $\tau_L = \hbar\omega_L S_s/\sigma W$, where ω_L is the frequency, W is the power, S_s is the cross section of volume irradiated, and σ is the cross section of light absorption, equal to 0.3 cm² and 2×10^{-17} cm², respectively; σ is derived from the extinction coefficient. These parameters result in $\sim 10^{-9}$ s for τ_L, within the experimental time resolution and laser pulse duration.

(27) We do not discuss separately the analogous reactions, those described by eqs 11,12 and 15,16, that may occur after thermal equillibrium of the triplets had been established.

(28) (a) Wong, S. K.; Hutchinson, D. A.; Wan, J. K. S. *J. Chem. Phys.* **1973**, *58*, 985. (b) Atkins, R. W.; Evans, G. T. *Mol. Phys.* **1974**, *27*, 1633. (c) Pedersen, J. B.; Freed, J. H. *J. Chem. Phys.* **1975**, *62*, 1706. (d) Argenhofer, A.; Toporowicz, M.; Bowman, M. K.; Norris, J. R.; Levanon, H. *J. Phys. Chem.* **1988**, *92*, 7164. (e) Schlüpmann, J.; Salikhov, K. M.; Plato, M.; Jacgermann, P.; Lendzion, F.; Möbius, K. *Appl. Magn. Res.* **1991**, *2*, 117.

(29) Shushin, A. I.; Depew, W; M. C.; Wan, J. K. S. *Res. Chem. Intermed.* **1991**, *16*, 165.

(30) Fehler, D. L.; Emeis, C. A.; Futrell, R. P. *J. Chem. Phys.* **1971**, *54*, 4921.

(31) Levin, P. P.; Khudyakov, I. V.; Kuzmin, V. A. *J. Phys. Chem.* **1989**, *93*, 208.

(32) This value was derived from the known value at room temperature (ref 15) and the empirical viscosity–temperature diagram: Bretsneider, S. *Properties of Gases and Fluids*; Chimia: Moscow, 1966.

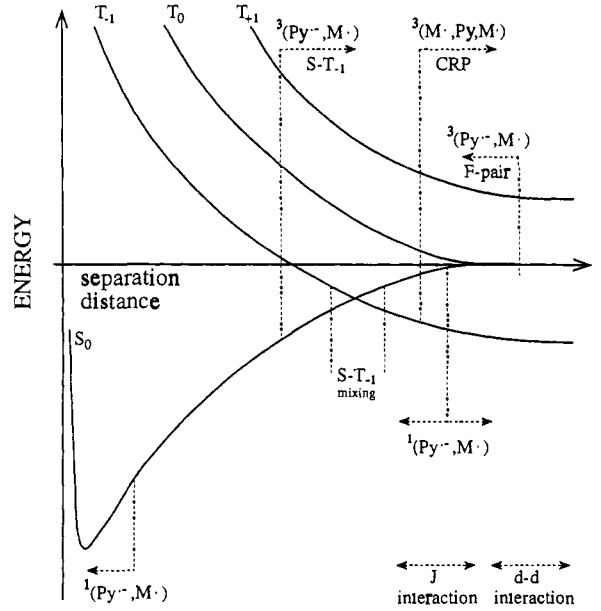

Figure 5. Energy of RP vs distance between its contituents (schematic dependence).

with the polarization of the medium.[33] The change of environment around such a localized electron resembles conventional solvation, but with the main difference that repulsion and not attraction alters the medium. Although the cation M^+ plays a minor role in the EPR detection, it induces a Columbic interaction between the constituents of the complex. Thus, the overall behavior of M• exhibits an ionic character, which should affect the polarization via diffusional motion.

The time evolution of the RP can evoke different ESP mechanisms, namely the S–T_0 RPM (including G- and F-pairs), S–$T_\pm$ RPM, and CRPM. We will illustrate these effects by means of Figure 5, where the schematic dependence of energy versus distance between the RP constituents is displayed.

C4. Correlated Radical Pair Mechanism. Restricted diffusion conditions are formed in a wide variety of systems such as the *in vivo* photosynthetic apparatus,[34] viscous solutions,[2c,28d,29] micelles,[3] and biradical systems.[4] The system discussed here, however, demonstrates the case where restricted diffusion can be achieved in nonviscous solution due to the Coulombic interaction between the radical species within the complex. The triplet RP, which is suggested to result in the observed CRP, is ^{3}(M•,Py,M•). The centered-field spectra, shown in Figures 2 and 3b, at τ_d = 24 ns originate from:

$$^1(M^\bullet,Py,M^\bullet) \overset{S\text{–}T_0}{\leftrightarrow} {}^3(M^\bullet,Py,M^\bullet) \qquad (18)$$

The A/E pattern (in frequency units) confirms a triplet precursor (assuming $J < 0$), which is in line with the CIDEP rules for $\Gamma = \mu J$:[1]

$$\Gamma > 0 \rightarrow E/A \quad \text{and} \quad \Gamma < 0 \rightarrow A/E \qquad (19)$$

where $\mu > 0$ for a triplet precursor and $\mu < 0$ for a singlet precursor. The magnetic parameters of the M• radicals may differ slightly if the degree of excitation for each radical is different. Such a difference is a consequence of different distances between M^+ and e^- within M•.[22] A different way to describe the origin of the S–T_0 mixing of the nearly identical electron-like radicals, M•, is the random electron jumps within the loose ion pair (see eq 6). Although the average hfc-value is small, one of the states between jumps possesses a very large hfc, which is close to the value for free alkali metal atom (ranging from 230 MHz for K to 2295 MHz for Cs).[23a] Thus, under restricted diffusion conditions, this effect can provide an effective and modulated difference in the hyperfine energies of the two radicals, M•. As shown in Appendix I for the RP ^{3}(M•,Py,M•) with nearly identical radical constituents, only two out-of-phase transitions, which are separated by $4J$, are observed.

Upon the RP formation, the RP undergoes an exchange interaction of $\sim 10^6$ rad/s (obtained from the experimental spectra with $\Delta\nu_{pp}$ = 0.7 MHz) that is usually expressed in the form of:[35]

$$J(r) = J_0 \exp(-\alpha r) \qquad (20)$$

where r is a separation distance between the RP constituents, $J_0 = (1.5\text{–}4.5) \times 10^{18}$ rad/s, and α = 2.2–2.7 Å^{-1}.[35] Within this approximation, the distance between two alkali metal atoms in the CRP is of the order of 10–13 Å. This number agrees well with the structure of solvent-separated Li complex shown in Figure 4.[35b] It should be reemphasized that the solvated electron, which is part of the monomer M•, possesses a sizable cavity. This explains why the interradical distance for contact complexes, e.g., (Cs•,Py,Cs•), could be very close to the one of solvent-separated complexes, e.g., (Li•,Py,Li•). Figure 5 shows the S–T energy separation of the RP vs distance between the RP constituents. The initial position of the CRP (M•,Py,M•) upon formation via ET processes (eqs 11–12, 18) is indicated at a distance related to the above discussion and correlates with the energy scheme in Figure 7. In addition, we should mention that a plausible mechanism of S–T_0 mixing may be due to a "sudden" change of the exchange interaction from $2J$ value ($\sim 10^6$ rad/s) at a distance where CRP prevails, to a vanishing value at a large distance, where S and T_0 states are degenerate (cf. Figure 5). Under such circumstances, the exchange interaction is a sharp function of time, and the slow adiabatic change may not be valid, resulting in of a mixture of different S and T_0 states.[1]

Diffusion of the constituents within the CRP produces the polarized species, $M^\bullet_A$, which exhibit CIDEP effects:

$$^3(M^\bullet,Py,M^\bullet)_p \overset{diff}{\rightarrow} M^\bullet_A + (Py,M^\bullet_A) \quad (\text{or } M^\bullet_A + Py + M^\bullet_A) \qquad (21)$$

The absorptive single line is clearly seen in the second time slices of Figures 2 and 3b.

C5. S–T_{-1} RPM and Radical–Triplet Pair Mechanism (RTPM). With the exception of Py/K/THF, the pure emissive spectra of $Py^{\bullet-}$ observed in the time interval of $2\text{–}5 < \tau_d < 50\text{–}100$ μs in all other systems (Figures 2 and 3b) can be caused by two simultaneous mechanisms: S–T_{-1} RPM[1] and radical–triplet pair mechanism (RTPM).[36] The former mechanism arises from the triplet precursor ^{3}(Py•−,M•), which is produced via the ET reaction 12. It can be further subdivided into two parts: (1) hyperfine-dependent and (2) hyperfine-independent. Thus, with S–T_{-1} mechanism and triplet precursor, the reaction proceeds to produce the two polarized species:

$$^3(Py^{\bullet-},M^\bullet) \overset{S\text{–}T_{-1}}{\rightarrow} Py^{\bullet-}_E + M^\bullet_E \qquad (22)$$

The time interval through which S and T_{-1} are almost degenerate is characterized by the separation distance shown in Figure 5. The S–T_{-1} mixing is operative either when the mixing

(33) (a) Dye, J. L. In *Progress in Inorganic Chemistry*; Lippard, S. J., Ed.; Wiley: New York, 1989; Vol. 32, p 327. (b) Jortner, J. *J. Chem. Phys.* **1959**, *30*, 839. (c) Nyikos, L.; Schiller, R. In *The Chemical Physics of Solvation*; Dogonadze, R. R., Kálmán, E., Kornyshev, A. A., Ultstrup, J., Eds.; Elsevier: Amsterdam, 1988; Part C, p 329.

(34) (a) Thurnauer, M. C.; Norris, J. R. *Chem. Phys. Lett.* **1980**, *76*, 557. (b) Hore, P. J.; Hunter, D. A.; McKie, C. D.; Hoff, A. J. *Chem. Phys. Lett.* **1987**, *137*, 495. (c) Norris, J. R.; Morris, A. L.; Thurnauer, M. C.; Tang, J. *J. Chem. Phys.* **1990**, *92*, 4239.

(35) (a) De Kanter, F. J. J.; Kaptein, R. *J. Am. Chem. Soc.* **1982**, *104*, 4759. (b) The α-value of 2.5 Å^{-1} has been calculated for a pair of hydrogen atoms (Herring, C.; Flicker, M. *Phys. Rev.* **1964**, *A134*, 362) and was adopted for direct interaction between any radicals (Adrian, F. J. *J. Chem. Phys.* **1972**, *57*, 5107). For indirect interaction, Adrian's estimation for the hydrogen atoms resulted in ~ 1 Å^{-1} for the α-value. The α-values of 2.2–2.7 Å^{-1} determined in this work are in line with the above figure for the direct interaction.

(36) (a) Blattler, C.; Jent, F.; Paul, H. *Chem. Phys. Lett.* **1990**, *166*, 375. (b) Blattler, C.; Paul, H. *Res. Chem. Intermed.* **1991**, *16*, 201.

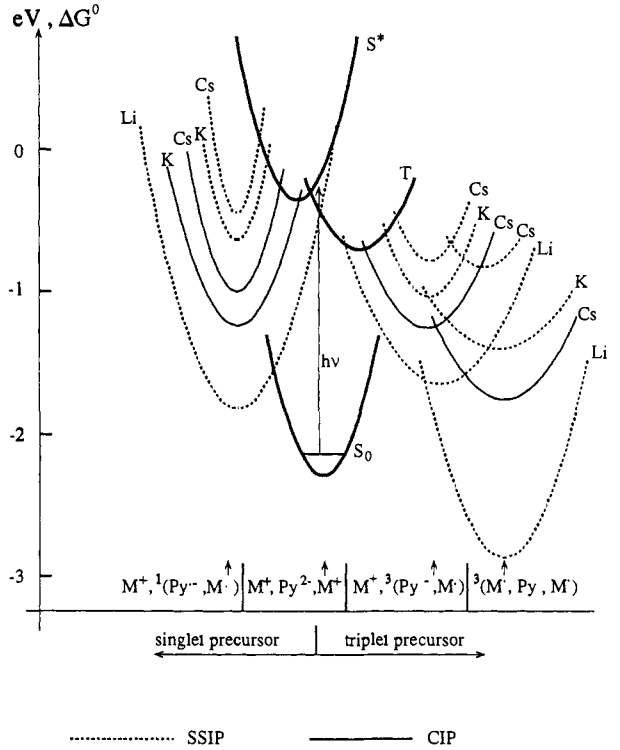

Figure 6. Free energy, $\Delta G°$ (calculated in Appendix II), vs reorganization coordinate (illustrated) for the different complexes that participate in the ET processes. SSIP (dotted curves) correspond to Py/M/THF (M = Li and Na) and to Py/M/THF,Kp for all alkali metals; CIP (solid lines) correspond to Py/M/THF (M = K, Rb, Cs). The potentials of Na and Rb systems behave properly but for simplicity reasons are not shown. The thick-line potentials correspond to the electronic states of Py^{2-}.

is sufficiently rapid (e.g., a large hyperfine coupling)[37] or when diffusion is considerably slow,[38] so that the time period of $S-T_{-1}$ degeneracy is extended, giving rise to an effective mixing. In our systems the hfc of $Py^{\bullet-}$ is small, whereas the one of the alkali metal atoms during electron jumps between the metal atom and the surrounding medium can be considerably bigger. In addition, in all systems the effective diffusion is highly restricted due to the cage effect.

Analysis of the experimental results indicates that no hyperfine component of the $Py^{\bullet-}$ spectrum vanishes. This is expected from conventional $S-T_{-1}$ polarization theory, in which the electron spin of $Py^{\bullet-}$ is coupled to its nuclear spins. We are left, therefore, with the $S-T_{-1}$ polarization, where the $Py^{\bullet-}$ spectrum does not depend on its own nuclear spin but depends on the nuclear spin of the counterradical, $M^{\bullet}$. This model is referred to as the $S-T_{-1}$ hyperfine-independent mechanism.[39] Therefore, if the $S-T_{-1}$ mixing is determined by the hfc of the counterradical, $M^{\bullet}$, then the characteristic mixing time, $\tau_{mix} = A^{-1} \approx 10^{-10}$ s (for $A \approx 100$ G), implies an effective mixing. However, the diffusion motion through the $S-T_{-1}$ mixing region occurs during the time interval $\tau_{diff} = \Delta r^2/D$, where Δr describes the characteristic dimension of the $S-T_{-1}$ mixing region. On the basis of the molecular dimensions (Figure 4), Δr can be estimated to be ~ 1 Å, and with $D \sim 10^{-8}$ cm^2/s, we have an estimate of τ_{diff} to be $\sim 10^{-8}$ s that satisfies the condition $\tau_{diff} \gg \tau_{mix}$. Similarly, τ_d can be estimated in the region where the $S-T_{-1}$ mechanism is operative. If the triplet RP $^3(Py^{\bullet-},M^{\bullet})$ triggers the $S-T_{-1}$ polarization with initial separation, r_0, equal to 2.2 Å for CIP and 6 Å for SSIP (cf. Figure

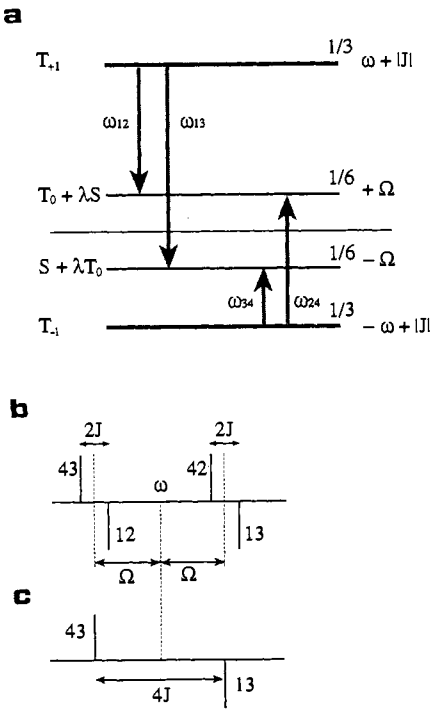

Figure 7. (a) Four-energy-level scheme of CRP. (b) Stick FT-EPR spectrum of CRP. For notations, see Appendix I. (c) Stick FT-EPR spectrum of CRP for identical radicals, where $\Delta\omega^2 \ll J^2$.

4), and the $S-T_{-1}$ mixing region position, $r_{S-T_{-1}}$, is at ~ 10 Å (Figure 5), a value of about 5 μs is calculated for τ_d (= $(r_{S-T_{-1}} - r_0)^2/D$), which is in line with our experimental observations.

In addition to the mechanism discussed above, a recently proposed mechanism[36] of net polarization can compete with the $S-T_{-1}$ RPM. This mechanism of net polarization was proposed in systems where net emissive polarized EPR spectra of radicals were observed for a period of 50 μs, with a zero signal at the beginning, having maximum polarization at 10–20 μs. Incidentally, this behavior is very similar to that observed in our systems (cf. Figures 2 and 3b). It was proposed that the mechanism of such ESP (RTPM) resembles F-pair RP mechanism but occurs during encounters of thermal triplet molecules with radicals producing doublets and quartets:[36,40]

$$M^+,{}^3(Py^{2-}),M^+ + Py^{\bullet-} \rightarrow {}^2[(M^+,{}^3(Py^{2-}),M^+),Py^{\bullet-}] \xrightarrow{\text{quenching}} {}^2[(M^+,{}^1(Py^{2-}),M^+),Py^{\bullet-}] \quad (23)$$

$$M^+,{}^3(Py^{2-}),M^+ + Py^{\bullet-} \rightarrow {}^4[(M^+,{}^3(Py^{2-}),M^+),Py^{\bullet-}] \xrightarrow{\text{diff}} Py^{\bullet-}{}_E + M^+,{}^3(Py^{2-})_p,M^+ \quad (24)$$

Whereas process 23 produces, due to quenching, the unpolarized doublet radicals, process 24 results in the quartet state. This leads to quartet–doublet mixing by the ZFS tensor. The splitting between the energy levels is set by the exchange interaction. In this case the polarization is[36]

$$P_{RTPM} \sim \omega J D^2{}_{ZFS} \quad (25)$$

where ω is the microwave frequency and $J = E(\text{doublet}) - E(\text{quartet})$. The RTPM assumes that rotational motion of the triplet molecule, which controls relaxation within its sublevels, is not very fast and is compared with the time interval of ZFS action. Therefore, high viscosity, low temperature, and high degree of solvation should increase the probability of RTPM. The long-lived equilibrated triplet state, which lasts for milliseconds,[41] certainly supports the existence of RTPM.

(37) (a) Verma, N. C.; Fessenden, R. W. *J. Chem. Phys.* **1976**, *65*, 2139. (b) Trifunac, A. D.; Nelson, D. J.; Mottley, C. *J. Magn. Reson.* **1978**, *30*, 263. (c) Adrian, F. T.; Akiyama, K.; Ingold, K. A.; Wan, J. K. S. *Chem. Phys. Lett.* **1989**, *155*, 333.

(38) (a) Trifunac, A. D. *Chem. Phys. Lett.* **1977**, *49*, 457. (b) Trifunac, A. D.; Nelson, D. J. *J. Am. Chem. Soc.* **1977**, *99*, 289.

(39) Buckley, C. D.; McLauchlan, K. A. *Chem. Phys. Lett.* **1987**, *137*, 86.

(40) Steiner, U. E.; Ulrich, T. *Chem. Rev.* **1989**, *89*, 51.

(41) Almgren, M. *Photochem. Photobiol.* **1967**, *6*, 829.

In the case of RTPM, the long-lived emission is due to slow production of thermal $Py^{\bullet-}$ or slow diffusion-controlled encounters of thermal species in eq 24. The rise time in this model is controlled by the relaxation time of the radical polarization, produced at earlier times (eqs 15 and 16, or 22) with spin-lattice relaxation time of 10–20 μs and/or by the diffusion-limited encounter time, $\tau_{bim} = \{4\pi Dr_0[M^+,^3(Py^{2-}),M^+]\}^{-1}$ estimated to be of the order of 20–40 μs (for $D \sim 10^{-6}$ cm^2 s^{-1} and concentration of the order of 10^{16} spins/cm^3). In both cases, the characteristic time is in line with the experimental lifetimes of the emissive polarization.

To conclude this section, interpretation of the results in the time period of 5–50 μs was carried out in the framework of two successive mechanisms: (1) S–T_{-1} RPM and (2) RTPM. In other words, the relaxed products of the ST_{-1} RPM (eq 22) serve as precursors for the RTPM (eq 24). Finally, we mention that the contribution of $M^{\bullet}_E$ is suppressed by the more intense absorptive spectra of the relaxed species of the CRPM.[42]

C6. S–T_0 RPM (G- and F-pairs). Inspection of Figure 3a clearly shows a basic difference between previously discussed spectra and those obtained in Py/K/THF solutions. Whereas the initial spectra in all other systems are characterized by a single A/E line superimposed on an absorption spectrum of $Py^{\bullet-}$, the spectrum of this system is characterized by a single emissive line superimposed on a multiplet E/A spectrum of $Py^{\bullet-}$. The interpretation of the time-evolved spectra of photoexcited Py/K/THF solutions will be carried out within the framework of S–T_0 RPM.

Primary ET forms the singlet RP, followed by S–T_0 mixing and diffusion:

$$K^+,^1(Py^{2-})^*,K^+ \xrightarrow{ET} {}^1(K^{\bullet},Py^{\bullet-}),K^+ \overset{S\text{–}T_0\,(J)}{\leftrightarrow} {}^3(K^{\bullet},Py^{\bullet-})K^+ \xrightarrow{diff} (K^+,Py^{\bullet-})_{E/A} + K^{\bullet}_E \quad (26)$$

Assuming that J is negative and utilizing the CIDEP rule (eq 19), the precursor for the observed multiplet and single-line spectra in the first two slices of Figure 3a is the singlet state (eq 26). The multiplet effect is typical of the S–T_0 mechanism applied to any RP obeying the Buckley–McLauchlan theorem,[43] which states that the EPR line intensity of the hyperfine component of one radical is 0 at the center of the spectrum of the other radical and vice versa. At the point of zero intensity, the spectra change phase. This effect is clearly shown in Figure 3a, where the spectrum of $Py^{\bullet-}$ changes its polarization phase at the frequency where the single-line spectrum (of $M^{\bullet}$) appears.

The phase inversion of the EPR spectra above $\sim$5 μs of both the single line and the multiplet warrants further discussion. If reaction 26 is valid, i.e., there is a singlet precursor for E/A polarization, then the relaxed radicals can reencounter to produce polarization via an F-pair mechanism:

$$K^+,Py^{\bullet-} + K^{\bullet} \xrightarrow{F\text{-}pair} K^+,^3(Py^{\bullet-},K^{\bullet}) \xrightarrow{diff} (K^+,Py^{\bullet-})_{A/E} + K^{\bullet}_A \quad (27)$$

This mechanism is very close to S–T_0 RPM for G-pairs, with the exception that the S–T_0 mixing occurs for the uncorrelated (free encounter) radicals.[1a] Obviously, one-fourth of the encounters produce singlet RP which recombine, and three-fourths of the encounters give rise to S–T_0 RPM with a triplet precursor. This mechanism should produce inverted spectra at longer times, as is shown in Figure 3a. The encounter rate, $k_F[R_1][R_2]$, for uncorrelated radicals R_1 and R_2 is expressed by $4\pi Dr_{S\text{–}T_0}[R_1][R_2]$, where D is the conventional diffusion coefficient and $[R_1]$ and $[R_2]$ are the concentrations of the encounter radicals. In this case, however, diffusion is not restricted due to the large interradical distance ($r_{S\text{–}T_0} > 13$ Å). For the diffusion-controlled (dc) reaction described by eq 27, τ_{dc} is calculated to be $\sim$100 μs ($\tau_{dc}^{-1} = k_F[R_2]$), which is appreciably larger than the experimental value of $\sim$5 μs (cf. Figure 3a). Therefore, additional mechanisms should be considered, which may account for the spectra obtained above 5 μs. In a mechanism proposed recently, it was suggested that the sign of CIDEP should correspond to the sign of the sum $J + V_{dd}$, where V_{dd} is the third-order contribution of the dipole–dipole interaction.[44] Dipole–dipole interaction is long range ($V_{dd} \sim 1/r^3$), and, consequently, at longer times, when the distance between the radicals becomes large, the exchange interaction (negative sign) can be neglected. Under such conditions, CIDEP is governed by V_{dd} (assumed to be positive), resulting in the sign change of CIDEP. This effect should be more conspicuous for systems with restricted diffusion.[44]

At this point we would like to answer the question why S–T_0 polarization appears immediately after the laser pulse. According to Figure 5 this should occur at large separation with a long delay time. The calculated distance between the electron spin of the metal radical and the delocalized electron spin on the pyrene radical varies from $\sim$2 to $\sim$9 Å (cf. Figure 4). It is most likely that the S–T_0 polarization, which is operative at early times (cf. Figure 3a), arises from those complexes having large interradical distance. These RPs diffuse out of the potential well at the S–T_0 mixing distances and obey the radical polarization immediately after the laser pulse (eq 26). Since the initial concentration of the RP is of the order of 10^{16} spins/cm^3, the polarization should be considerably high, even for a small fraction of the RPs produced out of the potential well. Because of the singlet character, the RPs within the potential well will recombine or undergo a back-ET:

$$K^+,^1(Py^{\bullet-},K^{\bullet}) \xrightarrow{recombination} K^+,^1(PyK)^- \quad (28)$$

$$K^+,^1(Py^{\bullet-},K^{\bullet}) \xrightarrow{back\ ET} K^+,^1(Py^{2-}),K^+ \quad (29)$$

The different manifestations of S–T_0 RPM, which are operative in the Py/K/THF system, and their dependence upon initial separation are illustrated in Figure 5. The overall mechanism takes into account that RPs possessing close initial separation recombine. Only a fraction of these RPs are formed out of the singlet well to exhibit a S–T_0 mixing. Further, RPs separate and can simultaneously undergo dipole–dipole interaction and the relaxation of polarized radicals.

Contrary to reaction with the triplet precursor, ET within the singlet with the formation of $^1(K^{\bullet},Py,K^{\bullet})$ does not occur. This is due to the recombination and back-ET (eqs 28 and 29). Those pairs which display S–T_0 polarization are formed at a separation distance of $\sim$12 Å, far from the contact distance, thus diminishing the ET probability. In addition, $^1(K^{\bullet},Py,K^{\bullet})$ should quickly recombine because of the singlet character of the precursor. The restrictions of having an ET process for the singlet pair do not exist in the analogous triplet complex which can undergo an ET. The ET in the triplet case is operative at a distance less than $\sim$6 Å (see above).

V. Electron-Transfer Mechanism

We will examine now which ET reactions are associated with the photoejection of the electron from Py^{2-} to the specific alkali metal cation. The basic ET processes can be formulated as follows:

$$M^+,(Py^{2-}),M^+ \rightarrow M^+,(Py^{\bullet-},M^{\bullet}) \quad (30)$$

$$M^+,(Py^{\bullet-},M^{\bullet}) \rightarrow (M^{\bullet},Py,M^{\bullet}) \quad (31)$$

The ET is driven by the Gibbs free energy difference between

(42) If RTPM is the only mechanism, the polarization of $M^{\bullet}$ does not appear at all. The $Py^{\bullet-}$ and $[M^+,^3(Py^{\bullet-},M^+)]$ species, which participate in the RTPM, are those generated by the current light pulse and those created in the preceding pulse and did not succeed in disappearing during the time between pulses. The spectral evolution of $Py^{\bullet-}$ at long times occurs simply within the spin relaxation time of $Py^{\bullet-}$ or by recombination (eqs 23 and 24).

(43) Buckley, C. D.; McLauchlan, K. A. *J. Magn. Reson.* **1984**, *58*, 334.

(44) Shushin, A. I. *Chem. Phys. Lett.* **1991**, *183*, 321.

the final and initial states, $\Delta G°$,[45,46] disregarding whether this arises from either Arrhenius-type thermal activation or tunneling mechanisms. Therefore, the ET rate and this energy gap are very sensitive to the factors that may affect the electron interactions between the reactants and products, such as center-to-center distance, shape and size of relevant species, orientational factors, solvation effects, nature of medium, etc. These considerations of ET rates vs free energy values are complicated but, nevertheless, are of basic importance in numerous chemical and biological systems.[46,47] Thus, it is worthwhile to estimate $\Delta G°$ for the different ET steps. This is to substantiate the proposed ET scheme, its energy scale, and its sequence with the different countercations. Such a derivation is carried out in Appendix II.

The driving forces in Figure 6 show that ET reactions 30 and 31 are thermodynamically allowed for all proposed complexes, i.e., SSIP for Li^+ and Na^+, and CIP for K^+, Rb^+, and Cs^+. The difference in the $\Delta G°$ values for the SSIP and CIP of the same alkali metal is associated with the simultaneous increase of the Coulombic interactions while the solvation energy is decreased upon the transition from SSIP type to CIP. One could expect that under the influence of chelating agents the solvation effect could be stronger, resulting in a large difference between the driving forces for SSIP and CIP, than in the case of conventional solvents.

The above consideration did not take into account the ionic character of $M^{\bullet} \equiv (M^+,e^-)$, which might affect the calculated driving forces. The estimation of $\Delta G°$ assumes that primary ET occurs from the S_2 state. This is based upon the MNDO calculation indicating that the second excited singlet, S_2, lies 2.3 eV above the ground state, S_0. This energy gap corresponds to the excitation wavelength, λ = 532 nm. Other routes such as internal conversion, $S_1 \leftarrow S_2$, should not affect the reaction sequence and its direction. Often, the excited CIP is manifested as a charge-transfer complex, i.e., this implies that the electron is partially shared by both ions.[48] This can induce strong orbital interactions between the complex constituents favoring their binding. Therefore, it can affect the driving force as well as restrict the diffusion within the cage.

The calculated results of Table III (Appendix II) do not indicate that the Py/K/THF system is different from all other systems. Nevertheless, there is no doubt that the experimental EPR results of the Py/K/THF suggest that only this system exhibits ESP patterns that originate from a singlet precursor (eq 26). This implies that only in the potassium CIP case, the ET is without activation, having a reorganization energy of $\lambda_s \approx -\Delta G°_s$:[49]

$$E_a = (\Delta G°_s + \lambda_w)^2/4\lambda_s \qquad (32)$$

Therefore, CIP with potassium represents a *unique* case, where the singlet potential curve of $[K^+,{}^1(Py^{\bullet-},K^{\bullet})]$ crosses the bottom of the curve of $[K^+,{}^1(Py^{2-})^*,K^+]$ (Figure 6). With this suggestion we may further assume that all other systems possess an activation energy (E_a).[49] The E_a values for Li^+, Na^+, Rb^+, and Cs^+ ion pairs with Py^{2-} will reduce the ET rates so that singlet-initiated ET cannot compete with the ISC rates to produce triplet radical pairs, $M^+,{}^3(Py^{\bullet-},M^{\bullet})$ and ${}^3(M^{\bullet},Py,M^{\bullet})$ (eqs 30 and 31). Within the framework of this model and Figure 6, ET involving the ground singlet state, S_0, of nonirradiated solutions is not feasible because of a large activation energy. Addition of the chelate, Kp, does not change the conditions for triplet-initiated ET channels. However, this small perturbation switches the singlet-initiated channel to the triplet-initiated one, evoking a dramatic change in the spectroscopy and kinetics of the photoexcited K/Py/THF system. This is in line with the zero-point crossing of the potential curves, where small perturbation should affect the reorganization energy (Figure 6).

VI. Conclusion

The analysis presented in this work and the comments on the ET reaction combined with Figure 6 suggest that the potential curves of Li and Na cross the potential curve of S* to the right of its minimum and that those of Rb and Cs cross it at the left. In addition, the dynamic behavior of these systems can be considered as novel and unique examples that combine within the same chemical system the properties of: (1) a fixed donor–acceptor distance due to the restricted diffusion, as implemented by the CRPM and (2) time evolution of the RP constituents to develop normal CIDEP effects. The remarkable similar CIDEP effects observed with Li, Na, Rb, and Cs (triplet-initiated) and the exceptionally different effects observed with K (singlet-initiated) strongly suggest that these alkali metal systems are novel examples of the inverted region in the Marcus theory.

The proposed mechanism of the photoinduced ET suggests that the competition between the ISC and ET rates dictates the precursor's character, i.e., singlet- or triplet-initiated reaction. This competition is responsible for the nonmonotonous dependence of the ET upon the $\Delta G°$. Moreover, since the ET occurs within quasistable complexes, it is not masked by a diffusion-controlled encounter process, which normally prohibits the observation of the Marcus inverted region or the bell-shaped $\Delta G°$ dependence of the ET rate in unorganized systems.[45,46,49,50] Moreover, the effect of chelating agent addition clearly lends support to the existence of such an inverted region for the systems under investigation and to the assumed model.

Acknowledgment. This work was supported by the Israel Council for Research and Development (V.R. and H.L.), U.S.-Israel BSF grants (H.L. and M.R.), a DFG grant (SfB 337, H.L.) and a special grant of the Erna and Victor Hasselblad Foundation (H.L.). The Farkas Research Center is supported by the Minerva Gesellschaft für die Forschung, GmbH, München, FRG. This work is in partial fulfillment of the requirements for a Ph.D. degree (G.Z.) at the Hebrew University of Jerusalem. The helpful suggestions made by Kobi Hasharoni and Dr. Dan Gamliel are highly appreciated. We are grateful to Prof. S. I. Weissman and Prof. J. R. Norris for their valuable comments.

Appendix I

Several theoretical treatments have been suggested to explain the antiphase pattern of the EPR signals.[3c,d,29,34c,51] They are based on the energy scheme presented for $J < 0$ in Figure 7a (where $2J = E_S - E_T$; E_S and E_T are the singlet and triplet energy states). The other definitions are the following:

$$\Omega^2 = J^2 + \Delta\omega^2_{ab} \qquad (AI\text{-}1)$$

$$2\Delta\omega_{ab} = \omega_1{}^a - \omega_2{}^b = \beta B(g_1 - g_2) + \sum A_{1n}{}^a M_{1n}{}^a - \sum A_{2m}{}^b M_{2m}{}^b \qquad (AI\text{-}2)$$

$$2\omega = \omega_1{}^a + \omega_2{}^b \qquad (AI\text{-}3)$$

where $\Delta\omega^2_{ab}$ is half the difference in the resonance frequencies, $\omega_1{}^a$ and $\omega_2{}^b$, of two hf states, a and b, of different radicals in the RP; the $A_{1n}{}^a$, $A_{2m}{}^b$ and $M_{1n}{}^a$, $M_{2m}{}^b$ are the corresponding hfc and

(45) Eberson, L. *Electron Transfer Reacitons in Organic Chemistry*; Springer-Verlag: Berlin, 1987.
(46) *Photoinduced Electron Transfer*; Fox, M. A., Chanon, M., Eds.; Elsevier: Amsterdam, 1988.
(47) *Electron Transfer in Organic, Inorganic and Biological Systems*; Bolton, J. R., Mataga, N., McLendon, G., Eds.; American Chemical Society: Washington, DC, 1991.
(48) Kavarnos, G. J. Photoinduced Electron Transfer I. *Top. Curr. Chem.* **1990**, *156*, 21.
(49) (a) Marcus, R. A. *Annu. Rev. Phys. Chem.* **1964**, *15*, 158. (b) Cannon, R. D. *Electron Transfer Reactions*; Butterworths: London, 1980. (c) Scandola, F. Photoinduced Electron Transfer II. *Top. Curr. Chem.* **1990**, *158*.
(50) Kakitati, T.; Yoshimori, A.; Mataga, N. In *Electron Transfer in Organic, Inorganic and Biological Systems*; Bolton, J.R., Mataga, N., McLendon, G., Eds.; American Chemical Society: Washington, DC, 1991; Chapter 4, p 45.
(51) Shushin, A. I. *Chem. Phys. Lett.* **1991**, *177*, 338.

magnetic quantum numbers referring to the n-th nucleus of radical 1 and the m-th nucleus of radical 2. The scheme displays the energy levels of the RP, which are derived using the basis set of singlet and triplet electron spin wave functions:

$$|1\rangle = T_{+1}\rangle,$$
$$|2\rangle = \cos\psi|S\rangle + \sin\psi|T_0\rangle,$$
$$|3\rangle = -\sin\psi|S\rangle + \cos\psi|T_0\rangle, \text{ and}$$
$$|4\rangle = |T_{-1}\rangle \qquad \text{(AI-4)}$$

$$tan(2\psi) = \Delta\omega_{ab}/J$$

This treatment also assumes that as in a conventional CIDEP theory, only S–T_0 mixing occurs i.e., $g\beta B \gg J$. For simplicity we assume that all of the precursor's triplet sublevels ($|T_{+1}\rangle$,$|T_0\rangle$,$|T_{-1}\rangle$) become equally populated as a result of photoexcitation. However, prior to RP formation, selective ISC may occur, causing a deviation from the one-third initially populated triplet state. In such a case, the observed spectra at early times conserve a triplet-precursor polarization built into the CRPM spectrum. Thus, an asymmetry in the two-phase pattern should occur, as is observed in our experiments (see Figures 2 and 3b). The transition frequencies are easily derived from Figure 7a:

$$\omega_{12} = \omega + |J| - \Omega \qquad \omega_{13} = \omega + |J| + \Omega$$
$$\omega_{42} = \omega - |J| + \Omega \qquad \omega_{43} = \omega - |J| - \Omega \qquad \text{(AI-5)}$$

Because of S–T_0 mixing, each of the states |2> and |3> possesses one-sixth overall population. The population differences induce the polarized EPR signals, with lines 43 and 42 in absorption and 12 and 13 in emission (cf. Figure 7b). In the CRP ^{3}(M•,Py,M•), both radicals possess nearly the same magnetic parameters, thus satisfying $\Delta\omega \ll J$ and, therefore, $\omega_{12} \approx \omega_{42}$. This results in that the two opposite polarizations cancel each other. Consequently, only transitions 43 and 13 are observed, with separation of $4J$ (cf. Figure 7c). Also, the cancellation of the absorptive and emissive transitions implies that $\Delta\omega < \Delta\omega_{1/2}$, where $\Delta\omega$ is the half-width.

Appendix II

The ET reaction in a donor–acceptor RP system obeys the scheme:

$$D^{m\bullet},A^n \rightarrow D^{m+1},A^{n-1} \qquad \text{(AII-1)}$$

where D and A denote the donor and acceptor and m and n are the respective charges. The driving force for this reaction is given by the energy balance in eq AII-2, where the donor's ionization potential, IP(D^m), and the acceptor's electron affinity, EA(A^n), related to the gas phase, replace the empirical oxidation and reduction potentials, usually used to estimate $\Delta G°$:[48,52]

$$\Delta G° = IP(D^m) - EA(A^n) - E_{00} + \sum\Delta G°_{sf} - \sum\Delta G_{si} + C_f - C_i \qquad \text{(AII-2)}$$

here, E_{00} is the 0–0 electronic energy of an excited donor state, $\Delta G°_{si}$ and $\Delta G°_{sf}$ are the solvation energies of the initial (reactants) and final (products) states (summation is required for SSIP and is carried out over all ions involved); and C_i and C_f are the Coulombic energies of the initial and final states. There are different expressions for SSIP and CIP to calculate the solvation energy. For SSIP, $\Delta G°_s$ is given by Born's equation:[53]

$$\Delta G°_s(SSIP) = -\sum_i (Z_i^2e^2/2a_{ef,i})(1 - 1/\epsilon) \qquad \text{(AII-3)}$$

where $a_{ef,i}$ is the effective ionic radius in the sphere approximation,

(52) Rehm, D.; Weller, A. Z. *Phys. Chem.* **1970**, *69*, 183; *Isr. J. Chem.* **1970**, *8*, 259.
(53) (a) Born, M. Z. *Phys.* **1920**, *1*, 45. (b) Chibisov, A. K. *Russ. Chem. Rev.* **1981**, *50*, 618. (c) Suppan, P. *Chimia* **1988**, *42*, 320.

Table I. Electron Affinities (EA), Ionization Potentials (IP), and Effective Radii (a_{ef})

	ion						
	Li^+	Na^+	K^+	Rb^+	Cs^+	Py^{2-}	$Py^•$
EA[a] (eV)	5.4	5.2	4.3	4.1	3.9		
a_{ef} (Å)	6[b]	6[b]	6[b]	6[b]	6[b]	3.1[c]	3.1[c]
IP (eV)						−2.7[d]	0.4[d]

[a] From ref 56. [b] Assuming that a_{ef} is approximately equal to the first solvent shell thickness, i.e., the diameter of THF molecule. [c] Assuming that the pyrene anions are partially solvated. [d] Calculated by MNDO.[18] [e] For systems with different alkali metals; the same shape, orientation, charge distribution, and dipole moment, which were calculated by MNDO for Li, are accepted.[18b]

Table II. Parameters Used for Calculating $-\Delta G°$ Values for ET Reactions

	ion pair[a]	
	M^+, Py^{2-}, M^+	$M^+, Py^{•-}, M^•$
μ, D	0.38[b]	5.7[b]
r_μ (Å)	3.1[c]	3.1[c]
$r_c(M–Py)^{SSIP}$ (Å)	6[d]	6[d]
$r_c(M–M)^{SSIP}$ (Å)	14[e]	
$r_c(M–Py)^{CIP}$ (Å)	2.0[f]	2.0[f]
$r_c(M–M)^{CIP}$ (Å)	6[b]	
a_c (Å)[7]	1.5	1.5

[a] See *e* in Table I. [b] See *d* in Table I. [c] Calculated from molecular volume in sphere approximation for molecular shape. [d] See *b* in Table I. [e] Calculated in accordance with Figure 4. [f] The distance between the M^+ and the localized charges in the aromatic ring (see Figure 4). [g] $a_c \approx (r_{M+} + d_{py})/2$, where r_{M+} is the radius of the alkali metal ion and d_{py} is the half-thickness of the aromatic ring.

Table III. $-\Delta G°$ Values[a] Calculated for ET Reactions

		alkali metal				
reaction		Li	Na	K	Rb	Cs
$M^+, Py^{2-}, M^+ \rightarrow M^+, Py^{•-}, M^•$	^{1}SSIP	1.7	1.5	0.6	0.4	0.2
	^{3}SSIP	1.5	1.3	0.4	0.2	0.0
	^{1}CIP			1.4	1.2	1.0
	^{3}CIP				1.0	0.8
$M^+, Py^{•-}, M^• \rightarrow M^•, Py, M^•$	^{3}SSIP	1.5	1.3	0.4	0.2	0.0
	^{3}CIP				0.6	0.4

[a] In eV.

Z_i is the charge of the particular ion, i, and ϵ is the dielectric constant of the medium. The value of a_{ef} should include the first layer of the solvent molecules because of electrical saturation.[54]

The $\Delta G°_s$ value for a CIP possessing an effective radius r_μ and a dipole moment μ, is given by Kirkwood's equation:[55]

$$\Delta G°_s(CIP) = -(\mu^2/r_\mu^3)[(\epsilon - 1)/(2\epsilon + 1)] \qquad \text{(AII-4)}$$

The Coulombic term is given by:[53c]

$$C = \sum_{i\neq j} Z_iZ_je^2[a_c/r_c^2n^2 + (1/\epsilon r_c)(1 - a_c/r_c)] \qquad \text{(AII-5)}$$

where Z_i and Z_j are the charges of the interacting particles and n is the refractive index of solute molecules. Other notations and the averaged values of the parameters which were used for calculations are given in Tables I and II. In our case, the alkali metal cations are the acceptors and EA(M^+) = IP($M^•$). In addition, we utilize the values: $\epsilon = 11.5$,[15,32] $E_{00} = 2.3$ and 2.1 eV for the singlet and triplet channels, respectively of reaction 30 (according to MNDO calculation[18] for Py^{2-}), and $n^2 \approx 2$.[53c] The $\Delta G°$ values are presented in Table III. All the values were calculated with an accuracy of 0.1 eV.

(54) Purcell, K. F.; Blaive, B. In *Photoinduced Electron Transfer*; Fox, M. A., Chanon, M., Eds.; Elsevier: Amsterdam, 1988; A, p 123.
(55) (a) Kirkwood, J. G. *J. Chem. Phys.* **1934**, *2*, 351. (b) Bootcher, C. J. F. *Theory of Electric Polarization*; Elsevier: New York, 1952.
(56) *CRC Handbook of Chemistry and Physics*, 60th ed.; Weast, R. C. Ed.; CRC Press: Boca Raton, FL, 1979-80; p F-214.